Methane dehydro-aromatization over Mo/MCM-22 catalysts: a highly selective catalyst for the formation of benzene

Yuying Shu, Ding Ma, Longya Xu, Yide Xu * and Xinhe Bao *

State Key Laboratory of Catalysis, Dalian Institute of Chemical Physics, Chinese Academy of Sciences, 457 Zhongshan Road, PO Box 110, Dalian 116023, PR China

E-mail: xuyd@ms.dicp.ac.cn; xhbao@ms.dicp.ac.cn

Received 12 June 2000; accepted 20 September 2000

A molybdenum-modified MCM-22 catalyst has been used for methane dehydro-aromatization. The catalytic performance on this Mo/MCM-22 catalyst is featured by a higher yield of benzene and a lesser yield of naphthalene in comparison with that on a Mo/HZSM-5 catalyst under the same experimental conditions. Methane conversion of 10.0% and benzene selectivity of 80% over a 6Mo/MCM-22 catalyst at 973 K was obtained. Based on the effect of contact time, it is suggested that the reaction is severely inhibited by the products, probably due to their strong adsorption and slow desorption. The Mo/MCM-22 catalysts were characterized by XRD, NH_3-TPD and TPSR techniques. XRD patterns of the Mo/MCM-22 catalysts confirmed that Mo species are highly dispersed on/in the MCM-22 zeolite if the Mo loading is less than 10%. NH_3-TPD experiment shows that the MCM-22 zeolite contains strong and exchangeable Brønsted acid sites. TPSR of methane revealed that there is an induction period during which the Mo species are reduced by methane and transformed probably into Mo_2C or $Mo_2O_xC_y$. It is concluded that the nature of the methane dehydro-aromatization reaction over the Mo/MCM-22 catalysts is similar to that on the Mo/HZSM-5 catalysts. The unique pore systems, the proper acid strength of the MCM-22 zeolite and the Mo species are factors important for methane dehydro-aromatization over Mo/MCM-22 catalysts.

Keywords: zeolite, MCM-22, Mo/MCM-22 catalyst, methane dehydro-aromatization, benzene

1. Introduction

Methane dehydro-aromatization over Mo/HZSM-5 catalysts in a continuous-flow mode has received attention recently [1]. Many catalysts have been evaluated, with the intention of finding ways to enhance the reactivity, stability and/or selectivity to aromatics in general and to light aromatics in particular. Most of the studies came to the same conclusion that the Mo/HZSM-5 catalyst is the best one among the tested catalysts. Solymosi et al. [2–5] evaluated many catalysts prepared from different Mo precursors and supports on the basis of H_2 and H_2O balances. Lunsford et al. [6,7] were the first to notice and analyze the production of naphthalene and to make quantitative correction for the coke formation on the Mo/HZSM-5 catalyst by an on-line GC analysis, using N_2 as an internal standard. Lin et al. [8] verified the internal standard method, using the data of material balance obtained from the analysis of the collected products from a bench scale reactor, with a catalyst charge of about 20 ml. At the same time, Lunsford et al. [6] and Solymosi et al. [3,5] indicated that there is an induction period during which the MoO_3 is reduced by CH_4 and transformed into Mo_2C. They suggested that the formed Mo_2C is responsible for methane activation. Meanwhile, the Brønsted acid sites of HZSM-5 are regarded to be responsible for the formation of aromatics. Ichikawa et al. also confirmed that Mo_2C was formed from their examination of the used catalyst by using the EXAFS technique [9]. Recently, Iglesia et al. suggested that $Mo_2O_xC_y$ in the channels also play a key role for the reaction [10–13].

Lunsford et al. examined various transition metal ions (TMI, such as Mo, Fe, V, W and Cr) and confirmed again that Mo is the best among the tested TMI [14]. More recently, Ichikawa et al. reported that rhenium-based HZSM-5 catalysts are also good catalysts for methane dehydro-aromatization [15].

The interaction between the Mo species and HZSM-5 is also of significance for a better understanding of methane dehydro-aromatization over Mo/HZSM-5 catalysts. Many techniques, such as NH_3-TPD, NH_4OH extraction, FT-IR, XPS, ion-scattering spectroscopy, NMR and EXAFS, have been used by several groups [1–7,9,16–21]. It appears that the original impregnated Mo species are mainly located on the external surface of the zeolite. After calcination at 773 K, however, part of the Mo species migrated into the channels which resulted in a decrease of the Brønsted acid sites. The Brønsted acid sites of MFI type zeolites also play a key role for the reaction since Mo/NaZSM-5 and/or Mo/Al_2O_3 catalysts only show little activity for the reaction [22,23]. Therefore, most of the researchers believe that the Mo/HZSM-5 is a bifunctional catalyst.

The reaction product distribution of the methane dehydro-aromatization is very complicated. In addition to light aromatics (mainly benzene) and naphthalene, there is also little amount of polyaromatics, as was confirmed by Ichikawa [24]. Therefore, the shape-selective function of the HZSM-5 zeolite may also play a crucial role during the

* To whom correspondence should be addressed.

reaction. Lin et al. recently tested the methane dehydro-aromatization over various Mo-based catalysts supported on different types of zeolites [25]. The authors correlated the catalytic performance to the structure of the zeolites, and came to the conclusion that the silica–alumina zeolites with a two-dimensional structure and a pore size approximating the dynamic diameter of benzene are good supports of the Mo-based catalysts for methane dehydro-aromatization.

It appears that till now, all the work reported by different research groups agreed that the best support is the HZSM-5 zeolite and that Mo is the best component among the tested TMI. Therefore, most of the research work on methane dehydro-aromatization is focused on the Mo/HZSM-5 catalyst.

Recently, a new high-silica zeolite, MCM-22, has been synthesized [26] and has found wide application for many hydrocarbon transformation processes [27–32]. This zeolite was first synthesized by Mobil Oil Corporation and has been reported to exhibit very high thermal stability and a high surface area. Corma et al. [33] have studied the void structure of MCM-22 by using model reactions such as the isomerization/disproportionation of m-xylene and the hydroisomerization of n-decane, and suggested that the MCM-22 zeolite has characteristics of both 10 MR and 12 MR zeolites. Lawton et al. [34] studied the framework topology of the MCM-22 and concluded that it has two independent pore systems with 10 MR apertures. Later, it was reported that MCM-22 zeolite catalysts modified by Zn and Ga are good catalysts for n-butane aromatization [35], and it is considered that methane dehydro-aromatization on Mo/HZSM-5 is an extension of light paraffin dehydro-aromatization on Zn- or Ga-modified HZSM-5 catalysts. Therefore, the unique pore structure of the MCM-22 zeolite may impose a particular effect on methane dehydro-aromatization. So far, no investigation of the MCM-22 zeolite has been reported in the literature concerning the methane dehydro-aromatization. In the present paper, the catalytic performance of a Mo-modified MCM-22 zeolite catalyst for methane dehydro-aromatization is reported.

2. Experimental

2.1. Catalyst preparation

The MCM-22 zeolite was synthesized using hexamethyleneimine (HMI) as a template and following the procedure described in [26]. A certain amount of sodium metaaluminate, sodium hydroxide (96% NaOH), R (about 85% HMI), silica (95% SiO_2) and deionized water were added into a vessel under vigorous stirring for 30 min. The resulting gel was then introduced into a stainless-steel autoclave, and heated to 423 K for some time until the gels crystallized completely. After quenching the autoclave in cold water, the sample was centrifuged at 5000 rpm, washed and dried at 383 K overnight. The chemical composition of the gel was as follows: $SiO_2/Al_2O_3 = 30$, $OH^-/SiO_2 = 0.18$, $Na/SiO_2 = 0.18$, $R/SiO_2 = 0.32$ and $H_2O/SiO_2 = 43$. The acid form of the MCM-22 was obtained by successive exchanging, and the SiO_2/Al_2O_3 ratio was 30, as determined by an XRF-1700 X-ray fluorescence spectroscope. The Mo/MCM-22 catalyst was prepared by an impregnation method according to the procedure as previously described in the preparation of the Mo/ZSM-5 catalyst [36]. Hereafter, Mo/MCM-22 catalysts were denoted as xMo/MCM-22, where x is the Mo content in weight percent.

2.2. Catalyst characterization

Specific surface area and average pore diameter of the samples were determined by the BET method basing on the adsorption isotherm at liquid nitrogen temperature, and using a value of 0.162 nm^2 for the cross-sectional area of N_2. The measurements were performed with an ASAP-200 Micromeritics equipment.

XRD patterns were obtained with a D/max-rb diffractometer using Cu Kα radiation at room temperature, with instrumental settings of 40 kV and 100 mA. The powder diffractograms of the samples were recorded from 5° to 40° at 5°/min scanning rate.

The morphology of the MCM-22 zeolite was observed by scanning electron microscopy (SEM). The zeolite samples were coated with gold prior to the SEM analysis to avoid the charge effect of the samples.

NH_3 temperature-programmed desorption (NH_3-TPD) was performed on a conventional set-up equipped with a thermal conductivity detector. 0.2 g of the sample was first flushed with He (30 ml/min) at 873 K for 30 min, then cooled to 423 K and saturated with NH_3 until equilibrium. It was then flushed with He again until the baseline of the integrator was stable. NH_3-TPD was then promptly started from 423 to 873 K at 15 K/min. All profiles were deconvoluted into two and/or three peaks by the Gaussian and Lorentzian curve-fitting method.

Temperature-programmed surface reaction (TPSR) of methane was carried out in a quartz tubular micro-flow reactor containing 0.15 g catalyst, using a Balzers QMS-200 multi-channel mass spectrometer for the monitoring of the reaction components. The catalyst was first heated to 873 K at a rate of 20 K/min in an Ar stream (40 ml/min) and held at 873 K for 30 min. Then it was cooled to room temperature. After this, the stream was switched from Ar to CH_4 (7.5 ml/min). Finally, the TPSR experiment was promptly started from room temperature to 1073 K at a heating rate of 5 K/min.

2.3. Catalyst evaluation

The reaction was carried out in a fixed-bed downflow reactor at 973 K and under atmospheric pressure. Briefly, 0.2 g of the catalyst and 2 g of quartz chips were charged into a 6.2 mm I.D. quartz tubular reactor. All the gases used were of UHP grade and used without further purification. The catalyst was first heated under a He stream

(15 ml/min) to 973 K and maintained at 973 K for 30 min, and then a 9.5% N_2/CH_4 gas mixture as the feed was introduced into the reactor at a space velocity of 1500 ml/g_{cat} h. By using N_2 as the internal standard, the methane conversion and the selectivity of the products, including the selectivity to carbonaceous deposits, can be calculated on-line on the basis of mass balance of carbon, as suggested by Lunsford et al. [6,7]. Hydrocarbon products including C_2 and condensable C_6–C_{10} aromatics such as benzene, toluene, xylene and naphthalene, etc., were separated and analyzed on-line by a gas chromatograph (Shimadzu GC-9AM) equipped with a column of OV-101 on the 6201 support and a flame ionization detector (FID). For on-line separation and analysis of H_2, N_2, CO, CH_4, CO_2, C_2H_4 and C_2H_6, etc., a HayeSep-D column and a thermal conductivity detector (TCD) were equipped on the same gas chromatograph. The reaction results were expressed in methane conversion, while the yields of the products and the selectivity to various products were calculated based on the consumed methane molecules.

3. Results and discussion

3.1. Catalyst characterization by XRD, SEM and BET

Figure 1 shows the XRD patterns of MCM-22 without and with different Mo loadings. The X-ray diffraction pattern of the as-synthesized MCM-22 sample shows almost the same feature as described in [26,35,37]. After modification by Mo, the corresponding patterns display only the characteristic peaks of MCM-22, and no MoO_3 crystallite patterns could be observed even for a Mo loading as high as 10%. The crystallinity of the MCM-22 zeolite decreased slightly with increasing Mo loading, as revealed by the patterns. This indicates that MoO_3 is highly dispersed on the MCM-22 surface and/or in its channels.

The SEM micrograph clearly shows that either the MCM-22 or the Mo/MCM-22 sample is in the form of thin platelet-like crystals, and no amorphous materials have been observed, as shown in figure 2.

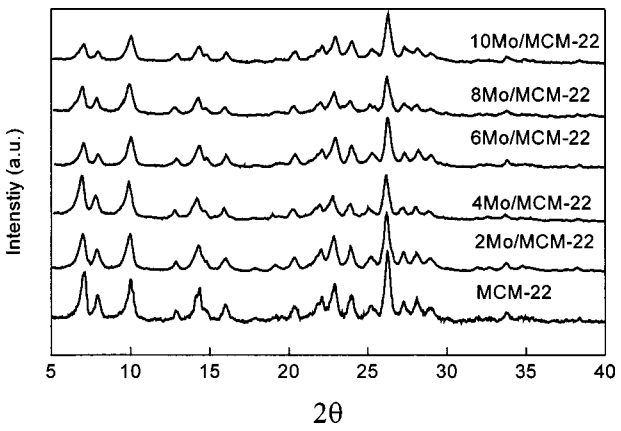

Figure 1. XRD patterns of the MCM-22 zeolite as synthesized and Mo/MCM-22 catalysts with different Mo loadings as prepared.

The BET and microsurface areas and micropore volumes for MCM-22 as well as for Mo/MCM-22 are listed in table 1. The BET surface area is 458 m^2/g while the micropore volume is 0.16 cm^3/g for MCM-22. These data are in reasonable agreement with those reported in [37–39]. With increasing Mo loading, the surface area and the micropore volume show an obvious decrease and the changes are in parallel with the crystallinity. This implies that the Mo species are well dispersed on the zeolite and that high Mo loading would block up the channels of the zeolite, leading to a decrease in the surface area and an increase in the average pore size.

3.2. Methane dehydro-aromatization over the Mo/MCM-22 catalysts

The effect of Mo loading on the catalytic performance was examined after running the reaction for 180 min, as shown in figure 3. Mo species are an important factor

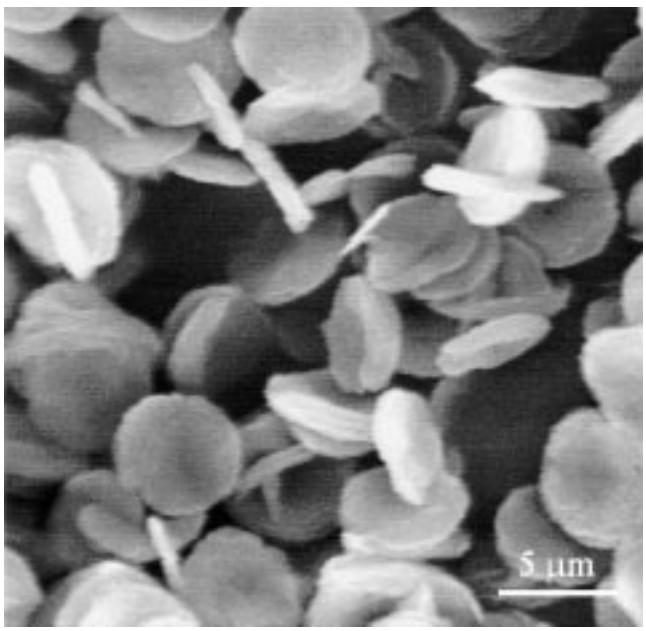

Figure 2. SEM image of as-synthesized MCM-22 zeolite. The ratio of the diameter to height of the crystal is about 8.

Table 1
BET surface areas, pore volumes and average pore diameters of various Mo/MCM-22 catalysts with different Mo loadings.

Sample	Surface area (m^2/g)	Micropore area (m^2/g)	Micropore volume (cm^3/g)	Average pore diameter (nm)	Ref.
MCM-22(30)			0.16		[31]
MCM-22(25)	400		0.16		[30]
MCM-22(28)	505		0.20		[32]
MCM-22(30)	458	352	0.16	1.97	This work
2Mo/MCM-22	417	322	0.15	2.12	This work
4Mo/MCM-22	418	312	0.14	2.32	This work
6Mo/MCM-22	398	306	0.14	2.30	This work
8Mo/MCM-22	393	288	0.13	2.33	This work
10Mo/MCM-22	357	273	0.13	2.22	This work

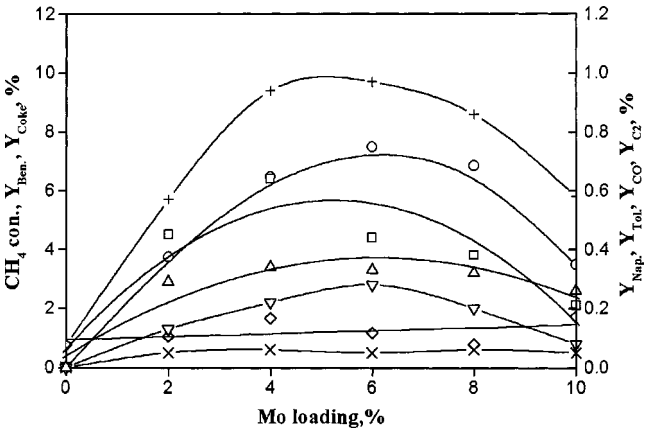

Figure 3. The effect of Mo loading on the catalytic performance after running the reaction for 180 min. (+) CH_4 conversion, (○) Y_{Ben}, (□) Y_{Nap}, (▽) $Y_{Tol.}$, (◇) Y_{Coke}, (△) Y_{C_2} and (×) Y_{CO}.

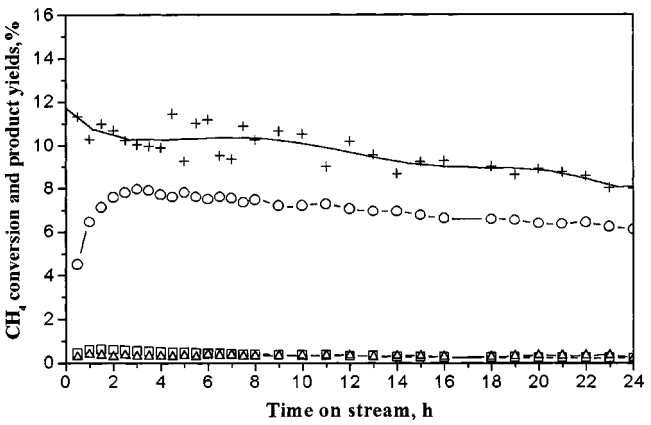

Figure 4. Changes of the methane conversion (+) and the yields of benzene (○), naphthalene (□) and C_2 (△) with the time on stream on the 6Mo/MCM-22 catalyst.

for methane dehydro-aromatization over the Mo/MCM-22. There is not any reaction activity for pure MCM-22 zeolite but only coke formed. The activity increases with the increase of Mo loading from 0 to 6% and reaches its maximum at a Mo loading of about 6%. Surprisingly, despite the fact that MCM-22 has a relatively high surface area, the methane conversion, X_{CH_4}, decreases quickly with the increase of the Mo loading from 6 to 10%. The changes in the yields of benzene, naphthalene and C_2 follow the same trend as X_{CH_4}, implying that all these three compounds may be formed via common intermediates and are the main products. The yield of carbonaceous deposits increases slightly with the Mo loading, indicating that in addition to the strong acid sites, Mo species are also responsible for the formation of carbonaceous deposits.

The changes in CH_4 conversion, X_{CH_4}, and product yields on the 6Mo/MCM-22 with on-stream time are shown in figure 4. Benzene formation reaches its maximum value after running for 180 min. The yield of benzene is obviously enhanced on the 6Mo/MCM-22 and the highest value is 8%, whereas the yield of naphthalene is remarkably suppressed and the highest value is less than 0.6% at

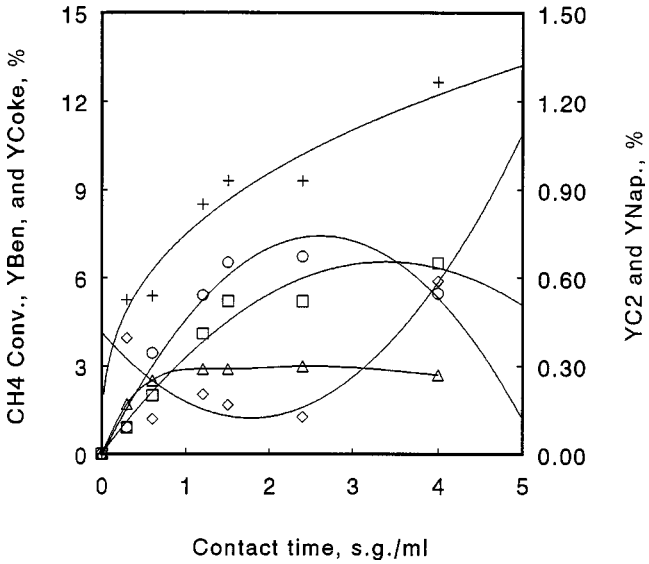

Figure 5. The effect of contact time on methane conversion (+) and the yields of benzene (○), naphthalene (□), carbonaceous deposits (◇) and C_2 (▽) after running the reaction for 90 min.

a methane conversion of about 10%. Meanwhile, the C_2 yield was kept at a low value and remained constant during the whole reaction period. It can be seen that the activity of the 6Mo/MCM-22 catalyst decreased slowly over a period of 24 h.

The effect of contact time on methane conversion and the yields of benzene, naphthalene, carbonaceous deposits and C_2 after running the reaction for 90 min are shown in figure 5. When the contact time was more than 1.2 s g/ml, the change of the contact time was realized by altering the flow rate of the feed and its change was realized by decreasing the charge of the catalyst while the contact time was less than 1.2 s g/ml. It is difficult to get a clear picture of the effect of contact time on the reaction due to the existence of the induction period in the early stage of the reaction as well as the significant formation of carbonaceous deposits. However, the change of the catalytic performance on the 6Mo/MCM-22 with the contact time may give us some important clues. It is apparent from the figure that the methane conversion does not follow a linear relationship with respect to the contact time. It increases sharply if the contact time is less than 0.5 s g/ml, and then more smoothly with the increase of the contact time. It means that methane dehydro-aromatization is severely inhibited by the products due to their strong adsorption and slow desorption on the catalyst surface, and their slow diffusion in the channels. This behavior can be attributed to the competition between methane and other hydrocarbon molecules for the active sites. It is interesting to notice the variance of the products yields, such as C_2, benzene, naphthalene and carbonaceous deposits with the contact time. The yields of C_2, benzene and naphthalene increase after passing through the origin, whereas the yield of carbonaceous deposit decreases with the increasing of contact time in the range of 0–0.5 s g/ml. It implies that carbonaceous deposits are the initial product

Table 2
A comparison of catalytic performances of Mo/MCM-22 and Mo/ZSM-5 catalysts under the same reaction conditions.[a]

Sample	Conversion of methane (%)	Selectivity (%)					Yields (%)	
		CO	C_2	Ben.	Nap.	Coke	Ben.	Nap.
2Mo/MCM-22	5.7	0.9	4.9	67.8	7.9	18.5	3.9	0.5
6Mo/MCM-22	10.0	0.2	3.4	80.0	4.4	12.0	8.0	0.4
10Mo/MCM-22	5.8	0.8	4.5	61.4	3.6	29.7	3.6	0.2
2Mo/ZSM-5	9.7	0.7	4.1	47.2	22.0	26.0	4.6	2.1
6Mo/ZSM-5	10.6	1.0	3.3	57.8	19.8	18.1	6.1	2.1
10Mo/ZSM-5	10.7	1.0	3.6	47.7	13.2	34.5	5.1	1.4

[a] Reaction temperature is 973 K, space velocity is 1500 ml/g h. All results were the values at optimum reaction stage, i.e., after 180 and 90 min of running for Mo/MCM-22 and Mo/HZSM-5 catalysts, respectively.

(which is in agreement with the formation of Mo_2C [3–7] or $Mo_2O_xC_y$ [10–13] in the early stage of the reaction), and that the products C_2, benzene, and naphthalene are the primary ones formed in parallel with each other or formed through the same reaction intermediate, i.e., the active carbon species. On the other hand, with further increase of the contact time (longer than 1.0, but less than 2.4 s g/ml) the yields of benzene and naphthalene still increase but the yield of C_2 remains constant. It suggests that with a longer contact time, the subsequent reaction of C_2 (mainly ethylene) to form benzene may occur. When the contact time is longer than 2.4 s g/ml, the yield of benzene decreases very quickly. In accordance with this, the yield of carbonaceous deposits increases steeply with the contact time. This suggests that at a longer contact time the condensation reaction of aromatics contributes to the formation of carbonaceous deposits.

A comparison of the catalytic performances of Mo/MCM-22 and Mo/ZSM-5 catalysts under the same experimental conditions was carried out and the results are listed in table 2. It is obvious that the catalytic performance on the Mo/MCM-22 catalyst is featured with higher selectivity to benzene and lower selectivity to naphthalene in comparison with that on the Mo/HZSM-5 catalyst. The 6Mo/MCM-22 catalyst exhibits excellent catalytic performance among the tested catalysts with different Mo loadings.

3.3. NH_3-TPD characterization of acid sites of the Mo/MCM-22 catalyst

Figure 6 shows the NH_3-TPD profiles recorded from the Mo/MCM-22 catalysts with different Mo loadings. Similar to the NH_3-TPD profiles of HZSM-5 reported in [36], two peaks, denoted as peak H and peak L and centering at about 681 and 532 K, respectively, exist on the NH_3-TPD profiles of the MCM-22 zeolite. The NH_3-TPD results of the MCM-22 in our experiment are reasonably consistent with the NH_3-TPD results of the MCM-22 having a SiO_2/Al_2O_3 ratio of 42, as reported by Unverricht et al. [40]. The authors claimed that there were three peaks located at 518, 627 and 834 K, respectively, after curve fitting for their NH_3-TPD

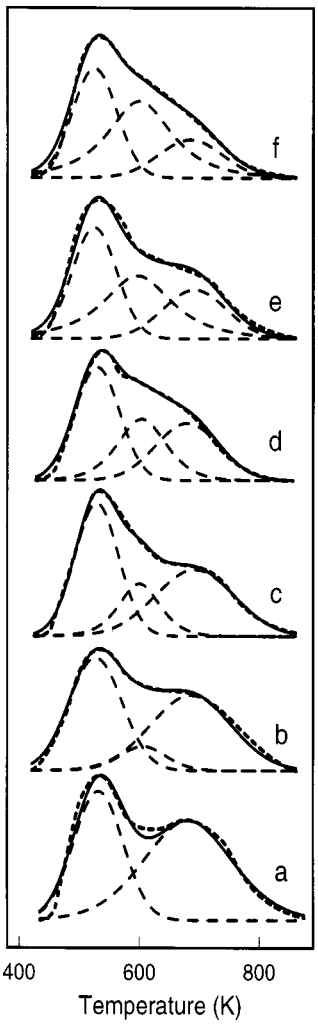

Figure 6. NH_3-TPD spectra of MCM-22 (a) and Mo/MCM-22 catalysts with different Mo loadings: 2 (b), 4 (c), 6 (d), 8 (e) and 10% (f).

profiles. The peak at 518 K was attributed to the desorption of the physisorbed NH_3 species and/or NH_3 adspecies residing on non-exchangeable cationic sites, while the peak at 627 K was assigned to the desorption of NH_3 adspecies adsorbed on exchangeable protonic sites, i.e., Brønsted acid sites. Finally, the peak at 834 K was attributed to strong Lewis acid sites. It is understandable that the difference in the peak temperatures may be resulted from the samples with different SiO_2/Al_2O_3 ratios and from different experimental conditions.

For the Mo/MCM-22 catalysts, the areas of both peak L and peak H decrease with the introduction of Mo, but the area of peak H decreases more obviously. Meanwhile, a new peak at about 600 K emerges, which is denoted as peak M. The area of peak M increases with the Mo loading, as can be seen from figure 6. This indicates that the impregnated Mo species can interact with the Brønsted acid sites and generate the medium-strength acid sites [41], and this kind of interaction is strengthened with the increase of the Mo loading. Table 3 lists the curve-fitting results of NH_3-TPD profiles recorded from the Mo/MCM-22 with

Table 3
Peak temperatures of NH_3-TPD spectra and the corresponding amounts of acid sites of Mo/MCM-22 catalysts with different Mo loadings.

Sample	Peak (L)		Peak (M)		Peak (H)	
	Peak temp. (K)	Area (arb. unit)	Peak temp. (K)	Area (arb. unit)	Peak temp. (K)	Area (arb. unit)
MCM-22	532	448	–	–	681	640
2Mo/MCM-22	527	425	606	82	686	435
4Mo/MCM-22	529	418	600	165	692	381
6Mo/MCM-22	529	362	604	226	680	261
8Mo/MCM-22	525	352	597	342	692	221
10Mo/MCM-22	525	345	600	390	685	173

different Mo loadings. The results suggest that the distribution of acid strengths on MCM-22 is different from that of HZSM-5, particularly in the region of strong acid sites. The latter has stronger acid sites than the former. The peak temperature for peak H is about 723 K for HZSM-5 [36] and is about 681 K for MCM-22. On the other hand, it can be found that with a Mo loading of 6%, the Brønsted acid sites decrease by 60%, indicating that the Mo species migrated into the channels and located closely to the Brønsted acid sites of the MCM-22 zeolite.

3.4. TPSR of methane over the Mo/MCM-22 catalyst

TPSR results of methane over the 6Mo/MCM-22 catalyst are shown in figure 7. A blank experiment with the MCM-22 sample under the same conditions showed that not any uptakes could be detected, and the response curve exhibited as a horizontal line. However, with the 6Mo/MCM-22 catalyst, there are two peaks in the response curve of CO_2, which imply that Mo^{6+} species were reduced in two stages. In the first stage, methane interacts with the Mo species to evolve CO_2 and H_2O, and the reduction of the Mo species is carried out smoothly. In the second stage, large amounts of CO and H_2 as well as little quantities of H_2O and CO_2 were produced simultaneously. Neither C_2H_4 nor C_6H_6 could be detected in these two stages. Only after the completion of CO_2 evolution at the temperature of 982 K could C_2H_4 and C_6H_6 evolve and their amounts became larger and larger. On the other hand, the evolution of CO and H_2O could still be detected. In fact, the profiles of TPSR of methane on the Mo/MCM-22 are similar to those on Mo/HZSM-5, as previously reported [42]. Since the reaction was carried out under non-oxidative conditions (no oxygen in the gas phase), the Mo species, which are coordinated with oxygen species, are the only oxygen source to be used to produce CO_2, CO and H_2O. Therefore, it is reasonable to propose that during the induction period, the Mo species of the Mo/MCM-22 catalysts will certainly be reduced and transformed into Mo_2C, as suggested by Lunsford et al. and Solymosi et al., or into $Mo_2O_xC_y$ as suggested by Iglesia et al. The reduction of the Mo species and its transformation into Mo_2C or $Mo_2O_xC_y$ are of importance for the formation of the active Mo species, which are responsible for the initial formation of hydrogen and benzene.

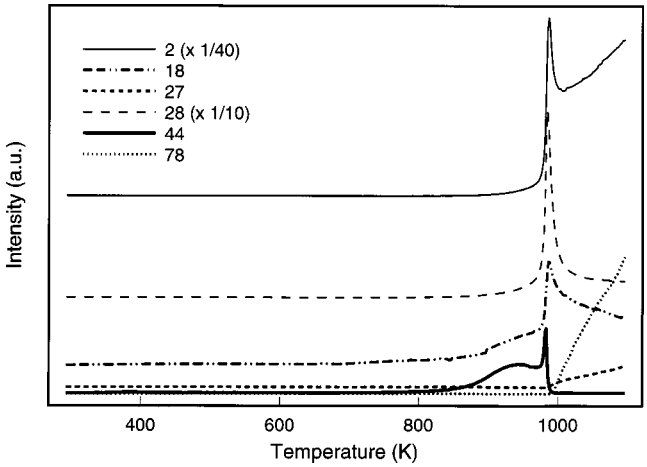

Figure 7. TPSR profiles of methane dehydro-aromatization over the 6Mo/MCM-22 catalyst: H_2 ($m/e = 2$), H_2O ($m/e = 18$), C_2H_4 ($m/e = 27$), CO ($m/e = 28$), CO_2 ($m/e = 44$) and C_6H_6 ($m/e = 78$).

4. Conclusions

The catalytic performance on the Mo/MCM-22 catalyst is featured with a higher yield of benzene and a lesser yield of naphthalene in comparison with those on the Mo/ZSM-5 catalyst under the same experimental conditions. Methane conversion of 10.0% and benzene selectivity of 80% over the 6Mo/MCM-22 catalyst at 973 K was obtained. XRD and BET measurements provided evidence that the Mo species are highly dispersed on/in the surface of the MCM-22 zeolite. The NH_3-TPD experiment shows that the MCM-22 zeolite contains exchangeable sites similar to the HZSM-5 zeolite. Meanwhile, TPSR in CH_4 stream revealed that Mo species were reduced in at least two stages before the formation of benzene. It is concluded that the formation of active Mo_2C species during the induction period and the nature of methane dehydro-aromatization on the Mo/MCM-22 catalyst may be the same as that on the Mo/HZSM-5 catalyst. The features of the catalytic performance of the Mo/MCM-22 catalyst are probably due to the unique 10-MR and 12-MR channel structure and pore arrangement of the MCM-22 zeolite. It can be concluded that the dispersed Mo species, the unique pore systems and the proper acid strength distribution of the MCM-22 zeolite all play important roles for methane dehydro-aromatization.

Acknowledgement

The authors thank the support of the National Natural Science Foundation of China and the Ministry of Science and Technology of China. The kind donation of a Mass spectrometer from Alexander von Humboldt-Foundation is gratefully acknowledged.

References

[1] Y. Xu and L. Lin, Appl. Catal. A 188 (1999) 53.
[2] F. Solymosi, A. Erdőhelyi and A. Szöke, Catal. Lett. 32 (1995) 43.
[3] F. Solymosi, A. Szöke and J. Cserényi, Appl. Catal. A 142 (1996) 361.
[4] F. Solymosi, A. Szöke and J. Cserényi, Catal. Lett. 39 (1996) 157.
[5] F. Solymosi, J. Cserényi, A. Szöke, T. Bansagi and A. Dszko, J. Catal. 165 (1997) 150.
[6] D. Wang, J.H. Lunsford and M.P. Rosynek, Topics Catal. 3 (1996) 289.
[7] D. Wang, J.H. Lunsford and M.P. Rosynek, J. Catal. 169 (1997) 347.
[8] Y. Lu, Z. Xu, Z. Tian, T. Zhang and L. Lin, Catal. Lett. 62 (1999) 215.
[9] S. Liu, L. Wang, Q. Dong, R. Ohnishi and M. Ichikawa, Stud. Surf. Sci. Catal. 119 (1998) 241.
[10] R.W. Borry III, E.C. Lu, Y.-H. Kim and E. Iglesia, Stud. Surf. Sci. Catal. 119 (1998) 403.
[11] R.W. Borry III, Y.H. Kim, A. Huffsmith, J.A. Reimer and E. Iglesia, J. Phys. Chem. B 103 (1999) 5787.
[12] Y.-H. Kim, R.W. Borry III and E. Iglesia, Micropor. Mesopor. Mater. 35–36 (2000) 495.
[13] W. Li, G.D. Meitzner, R.W. Borry III and E. Iglesia, J. Catal. 191 (2000) 373.
[14] B.M. Weckhuysen, D. Wang, M.P. Rosynek and J.H. Lunsford, J. Catal. 175 (1998) 338.
[15] L. Wang, R. Ohnishi and M. Ichikawa, Catal. Lett. 62 (1999) 29.
[16] Y. Xu, W. Liu, S. Wong, L. Wang and X. Guo, Catal. Lett. 40 (1996) 207.
[17] W. Liu, Y. Xu, S. Wong, J. Qiu and N. Yang, J. Mol. Catal. A 120 (1997) 257.
[18] W. Zhang, D. Ma, X. Liu, X. Liu and X. Bao, J. Chem. Soc. Chem. Commun. (1999) 1091.
[19] W. Zhang, D. Ma, X. Han, X. Liu, X. Bao, X. Guo and X. Wang, J. Catal. 188 (1999) 393.
[20] D. Ma, Y. Shu, W. Zhang, X. Han, Y. Xu and X. Bao, Angew. Chemie, in press.
[21] J.Z. Zhang, M.A. Long and R.F. Howe, Catal. Today 44 (1998) 293.
[22] L. Wang, L. Tao, M. Xie, G. Xu, J. Huang and Y. Xu, Catal. Lett. 21 (1993) 35.
[23] Y. Xu, S. Liu, L. Wang, M. Xie and X. Guo, Catal. Lett. 30 (1995) 135.
[24] R. Ohnishi, S. Liu, Q. Dong, L. Wang and M. Ichikawa, J. Catal. 182 (1999) 92.
[25] C. Zhang, S. Li, Y. Yuan, W. Zhang, T. Wu and L. Lin, Catal. Lett. 56 (1998) 207.
[26] M.K. Rubin and P. Chu, US Patent 4 954 325 (1990).
[27] R.M. Dessau and R.D. Partridge, US Patent 4 962 250 (1990).
[28] K.J. Del Rossi and A. Huss, Jr., US Patent 5 107 047 (1992).
[29] R.P.L. Absil, E. Bowes, G.J. Green, D.O. Marler, D.S. Shihabi and R.F. Socha, US Patent 5 085 762 (1992).
[30] C.T.W. Chu, T.F. Degnan and B.K. Huh, US Patent 4 982 033 (1991).
[31] C.T.W. Chu, US Patent 4 956 514 (1990).
[32] A. Corma, A. Martinez and C. Martinez, Catal. Lett. 28 (1994) 187.
[33] A. Corma, C. Corell, F. Lopis, A. Martinez and J. Perez-Pariente, Appl. Catal. A 115 (1994) 121.
[34] J.A. Lawton, S.L. Lawton, M.E. Leonowicz and M.K. Rubin, Stud. Surf. Sci. Catal. 98 (1995) 250.
[35] N. Kumar and L.E. Lindfors, Appl. Catal. A 147 (1996) 175.
[36] Y. Shu, Y. Xu, S. Wong, L. Wang and X. Guo, J. Catal. 170 (1997) 11.
[37] A. Corma, C. Corell, J. Perez-Pariente, J.M. Guil, R. Guil-Lopez, S. Nicolopoulus, J. Gonzalez-Calbet and M. Vallet-Regi, Zeolites 16 (1996) 7.
[38] A. Corma, V. Gonzalez-Alfaro and A.V. Orchilles, Appl. Catal. A 129 (1995) 203.
[39] R. Ravishankar, T. Sen, V. Ramaswamy, H.S. Soni, S. Ganapathy and S. Sivasanker, Stud. Surf. Sci. Catal. 84 (1994) 331.
[40] S. Unverricht, M. Hunger, S. Ernst, H.G. Karge and J. Weitkamp, Stud. Surf. Sci. Catal. 84 (1994) 37.
[41] K. Segawa and W.K. Hall, J. Catal. 76 (1982) 133.
[42] H. Jiang, L. Wang, W. Cui and Y. Xu, Catal. Lett. 57 (1999) 95.